molecules

MDPI

Article

Ab Initio Calculations on the Ground and Excited Electronic States of Thorium–Ammonia, Thorium–Aza-Crown, and Thorium–Crown Ether Complexes

Zhongyuan Lu, Benjamin A. Jackson and Evangelos Miliordos *

Department of Chemistry and Biochemistry, Auburn University, Auburn, AL 36849-5312, USA
* Correspondence: emiliord@auburn.edu

Abstract: Positively charged metal–ammonia complexes are known to host peripheral, diffuse electrons around their molecular skeleton. The resulting neutral species form materials known as expanded or liquid metals. Alkali, alkaline earth, and transition metals have been investigated previously in experimental and theoretical studies of both the gas and condensed phase. This work is the first ab initio exploration of an *f*-block metal–ammonia complex. The ground and excited states are calculated for $Th^{0–3+}$ complexes with ammonia, crown ethers, and aza-crown ethers. For Th^{3+} complexes, the one valence electron Th populates the metal's 6*d* or 7*f* orbitals. For $Th^{0–2+}$, the additional electrons prefer occupation of the outer s- and p-type orbitals of the complex, except $Th(NH_3)_{10}$, which uniquely places all four electrons in outer orbitals of the complex. Although thorium coordinates up to ten ammonia ligands, octa-coordinated complexes are more stable. Crown ether complexes have a similar electronic spectrum to ammonia complexes, but excitations of electrons in the outer orbitals of the complex are higher in energy. Aza-crown ethers disfavor the orbitals perpendicular to the crowns, attributed to the N-H bonds pointing along the plane of the crowns.

Keywords: thorium; multi-reference wave functions; solvated electrons; ammonia; crown ethers; aza-crown ethers; f-block; exited states; ab initio

check for updates

Citation: Lu, Z.; Jackson, B.A.; Miliordos, E. Ab Initio Calculations on the Ground and Excited Electronic States of Thorium–Ammonia, Thorium–Aza-Crown, and Thorium–Crown Ether Complexes. *Molecules* **2023**, *28*, 4712. https://doi.org/10.3390/molecules28124712

Academic Editor: Abdou Boucekkine

Received: 26 May 2023
Revised: 9 June 2023
Accepted: 9 June 2023
Published: 12 June 2023

Copyright: © 2023 by the authors. Licensee MDPI, Basel, Switzerland. This article is an open access article distributed under the terms and conditions of the Creative Commons Attribution (CC BY) license (https://creativecommons.org/licenses/by/4.0/).

1. Introduction

Isolated (gas phase) metal–ammonia complexes have been shown to host one or more diffuse electrons in their periphery [1,2]. Such complexes are called solvated electron precursors (SEPs) and the diffuse electrons reside at hydrogenic-type orbitals, which follow the energy order observed for the nuclear or Jellium shell models [1]. Specifically, the lowest-energy outer orbital is of s-type (dubbed 1s), followed by the 1p, 1d, 2s, 2p, and 1f orbitals [1]. This shell structure is universal and is independent of the central metal, including alkali metals, alkaline earth metals, boron, and transition metals [2–5]. The transition metal–ammonia complexes retain inner-valence *d*-orbitals of the metal [3,6–8]. Spectroscopic studies exist in the literature for lithium, sodium, magnesium, calcium, aluminum, vanadium, chromium, nickel, cobalt, copper, and silver [7,9–20]. In this work, we provide the first theoretical investigation of an *f*-block metal SEP, focusing on thorium–ammonia complexes.

Materials composed of SEPs (liquid or expanded metals) have been synthesized and characterized in detail for lithium [21,22], but have also been reported for multiple metals, including the lanthanides europium and ytterbium with the composition $Eu(NH_3)_6$ and $Yb(NH_3)_6$ [23]. Recently, such materials have been proposed as redox catalysts [24] and candidates for quantum information applications [25].

The first four ionization energies (IEs) of thorium (6.3067, 11.9, 20.0, and 28.8 eV) are remarkably lower than those of transition metals or other *f*-block elements [26]. For example, the same IE values for Eu, Yb, and V are in the ranges of 5.7–6.7, 11.3–14.6, 24.9–29.3, and 42.7–46.7 eV. Note that although the first two IEs are both comparable, the

third IE of thorium is about 5 eV lower, while its fourth IE is more than 15 eV lower and of the same order of the third IE of other metals. As will be explained later, this fact in combination with the large coordination numbers for its first solvation shell (up to ten) [27,28] render ammonia ligands capable of stabilizing highly oxidized metal centers and displacing multiple electrons of thorium to the periphery of the thorium–ammonia complex.

As shown later, a $Th(NH_3)_{10}$ is feasible with a Th^{4+} center and four diffuse electrons. This is the largest number of diffuse electrons observed so far. However, the most stable structure, $Th(NH_3)_8$, has a Th^{3+} center and three diffuse electrons. To see if this electronic structure is characteristic of ammonia coordination only, we used two aza-crown ether ligands with four and five nitrogen atoms each, thus retaining the number of nitrogen atoms anchored to the metal. Such complexes have been studied before for lithium, sodium, and magnesium [29]. Finally, we replaced the aza-crown ethers with the corresponding crown ethers (NH groups replaced by O atoms) to observe the effect of the coordinating atom and the presence of N−H bonds in the electronic structure of the complex.

In the next section, we detail the computational methods employed currently. Then we discuss our findings, and finally summarize our results.

2. Computational Details

The geometry optimizations were performed at the density functional theory (DFT) level using the CAM-B3LYP functional combined with the cc-pVDZ, cc-pVDZ, aug-cc-pVDZ, and cc-pVDZ-PP basis sets for carbon, nitrogen, hydrogen, and thorium centers, respectively [30–33]. The latter basis set is supplemented with the relative pseudopotential [34]. The employed functional was shown to provide accurate geometries of the MP2 and CCSD(T) level for other metal–ammonia complexes [35]. Gaussian 16 was invoked for these calculations [36]. Every optimized structure bears real harmonic vibrational frequencies; geometries and energies are given in the Supplementary Materials (SM).

The $Th(NH_3)_8{}^{4+}$, $Th(NH_3)_{10}{}^{4+}$, $Th(12C4N)_2{}^{4+}$, $Th(15C5N)_2{}^{4+}$, $Th(12C4O)_2{}^{4+}$ crown ether structures were used for the subsequent multi-reference calculations: 12C4X/15C5X denote aza-crown ethers with 12/15 the total number of non-hydrogen atoms and 4/5 the number of nitrogen (X=N) or oxygen (X=O) atoms. These species are closed shell, and they adopt the highest possible symmetry compared to the trications, dications, monocations, or neutral counterparts.

The active space for the CASSCF (complete active space self-consistent field) calculations generally includes both inner (6*d*, 7*f*) and outer (1s, 1p, 1d) diffuse orbitals, but has been adjusted to balance the computational cost based on the population of the various orbitals. For example, the inner orbitals are less and less populated when more electrons are added. The exact active space has been optimized by multiple trial-and-error attempts for each molecular species and is provided below accordingly. The subsequent CASPT2 (CASSCF + second-order perturbation theory) [37] calculations included the dynamic correlation from the ammonia/ammine/oxygen lone pairs as well. CASPT2 calculations have been shown to be sensitive to the used active space [38]. CASPT2 calculations with similar active spaces have been shown to agree perfectly with electron propagator techniques and EOM-CCSD calculations for other metal–ammonia complexes [1,3,39]. Due to the high computational cost, only the s and p functions of nitrogen and carbon centers from the cc-pVDZ sets are included. This is expected to have a minimal effect on computed excitation energies (<0.1 eV), as excitations occur only within the Th valence space and the peripheral orbitals of the complex, which are described predominantly by the hydrogen atom basis functions [40]. The MOLPRO suite of codes [41] is used, specifically, the internally contracted version of CASPT2 (CASPT2c) [42]. A level shift value of 0.2 a.u. and IPEA shift of 0.25 a.u. were used to resolve linear dependence issues [43].

3. Results and Discussion

We first optimized the geometries for the $Th(NH_3)_n{}^{4+}$ and $Th(NH_3)_n{}^{3+}$ species for n = 1–10. We considered only the isomers where all ammonia ligands are coordinated to

thorium. These systems have simple electronic structure (no or one unpaired electron) and are described properly with single determinantal methods such as DFT. The optimized geometries for trications are shown in Figure 1, along with the singly occupied molecular orbital (SOMO). for each structure. The ground state of Th^{3+} is $^2F(7f^1)$ and it stays in the ^2F state only for one ammonia ligand. After coordination of additional ammonias results in the population of a ~$6d_z{}^2$-type SOMO up to $n = 9$. For $Th(NH_3)_{10}{}^{3+}$, the SOMO becomes a ~$6d_{xz}$ type.

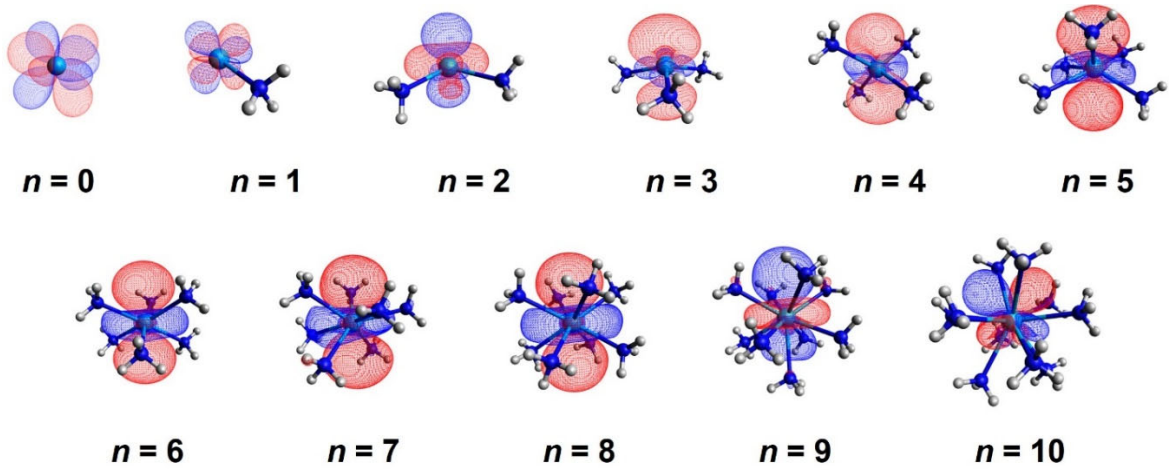

Figure 1. Optimized geometries and contours for the singly occupied orbital of $Th(NH_3)_n{}^{3+}$, $n = 0$–10.

The sequential dissociation energy D_e for the ammonia ligands, $Th(NH_3)_n{}^{4+,3+,0} \rightarrow Th(NH_3)_{n-1}{}^{4+,3+,0} + NH_3$ at CAM-B3LYP ($D_e = E[Th(NH_3)_{n-1}{}^{4+,3+,0}] + E[NH_3] - E[Th(NH_3)_n{}^{4+,3+,0}]$, where E[X] denotes the equilibrium energy of species X), is plotted with respect to n in Figure 2. We faced insurmountable technical/convergence issues for several cationic and dicationic species, likely due to their complex electronic structure (see below), and thus these species are not included in the figure. The ground state is a singlet and doublet for 4+ and 3+ charges, respectively, and is a singlet for $1 \leq n \leq 4$ and triplet for $5 \leq n \leq 10$ in the neutral complexes (see Supplementary Materials). The binding energy drops sharply with increase in n for the +4 charge (on average by 18 kcal/mol per ammonia ligand). For all species, but more evidently for the trications, there is a sudden drop going from $n = 8$ to $n = 9$. For the neutral, the D_e range is 15 ± 6 kcal/mol for $1 \leq n \leq 8$, which becomes 7.3 and 5.7 kcal/mol for $n = 9$ and 10, and there is a slight increase in D_e from $n = 7$ to $n = 8$ (9.8 to 13.0 kcal/mol). Therefore, we believe that the most prominent structure of a thorium expanded metal will be the octacoordinated $Th(NH_3)_8$, unlike the hexacoordinate $Eu(NH_3)_6$ and $Yb(NH_3)_6$ [23].

Using the $Th(NH_3)_8{}^{4+}$ structure (D_{4d} actual point group, C_{2v} computational point group), we performed CASSCF and CASPT2 calculations for all species with charges from 3+ to 0 in order to elucidate their electronic structure and explain the convergence issues in DFT for the intermediate charges (1+ and 2+). The geometry and CASSCF active orbitals for $Th(NH_3)_8{}^{3+}$ are depicted in Figure 3 and include the inner *6d* and *7f* orbitals of thorium and the outer 1s, 1p, and 1d of the whole complex ($1e^-/21$ orbitals). The energies for the $1s^1$, $1p^1$, $1d^1$, $6d^1$, and $7f^1$ states are listed in Table 1. The lowest energy states, $\tilde{X}^2A_1$, 1^2E_2, and 1^2E_3, correspond to *6d* orbitals of thorium. The ground state has a $(6d_z{}^2)^1$ configuration and is well separated from the other *6d* states and higher excited states by $\geq$1.3 eV. The first few *7f* states (1^2B_2 and 1^2E_1) appear next at ~2.0 eV, followed closely by the first electronic state with an outer electron (2^2A_1; $1s^1$). At ~1.0 eV higher are the $1p^1$ states (2^2B_2, 2^2E_1) and one more degenerate *7f* state (2^2E_2). The last *7f* state is at ~3.5 eV. All outer 1d states lie between 4.2 and 4.9 eV. Note that the CASSCF and CASPT2 excitation energies differ by less than 0.17 eV.

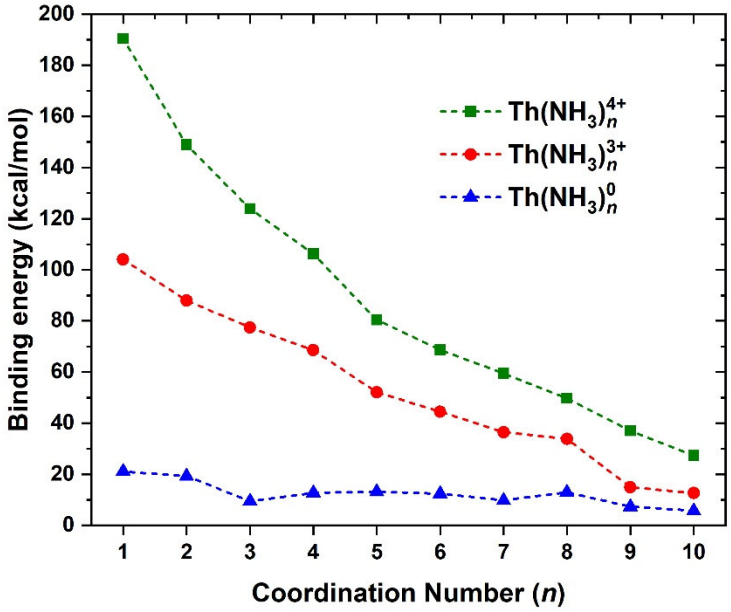

Figure 2. Dissociation energy (D_e) for ammonia ligands in the $Th(NH_3)_n^{4+,3+,0}$ complexes corresponding to the $Th(NH_3)_n^{4+,3+,0} \rightarrow Th(NH_3)_{n-1}^{4+,3+,0} + NH_3$ dissociation process.

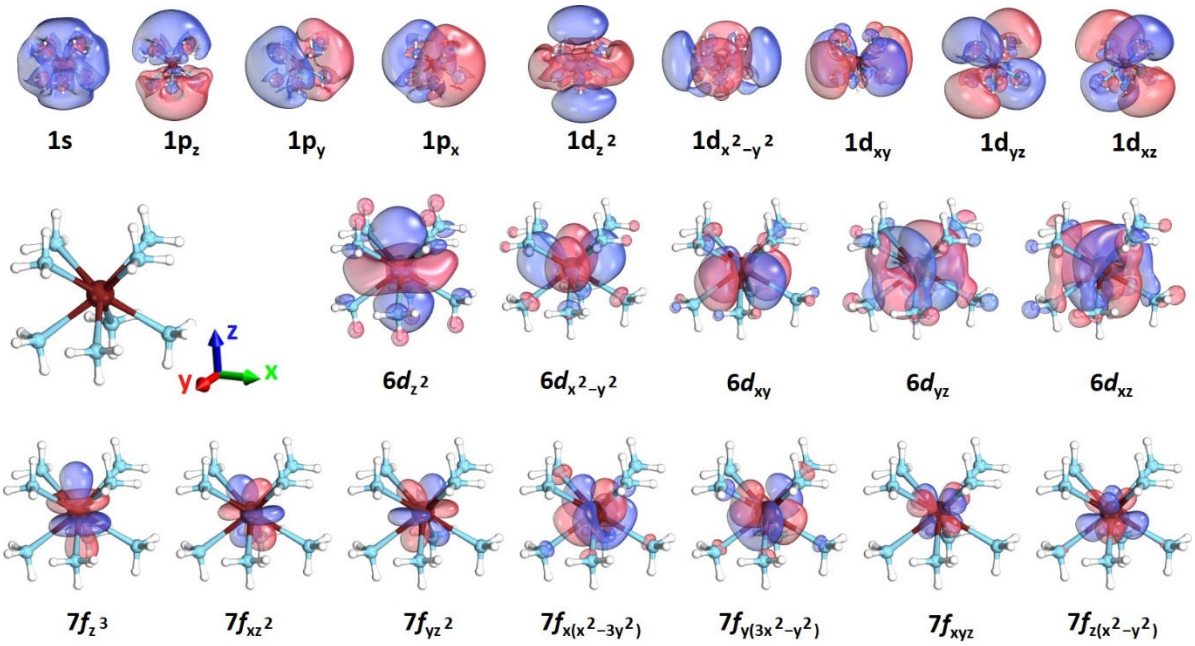

Figure 3. Geometry of $Th(NH_3)_8^{4+}$ and CASSCF active orbitals for $Th(NH_3)_8^{3+}$; 1s, 1p, 1d correspond to peripheral outer orbitals, and 6*d*, 7*f* to inner thorium orbitals.

The addition of one more electron results in a highly multi-reference wave function, explaining the convergence issues with DFT. CASSCF calculations ($2e^-/15$ orbitals) of the dication includes two electrons in fifteen orbitals (1s, 1p, 1d, $6dz^2$, and five orbitals of $7f/6d$ character). The results show the ground state $\widetilde{X}^1A_1$ of $Th(NH_3)_8^{2+}$ has two major electronic configurations, $\left|\widetilde{X}^1A_1\right\rangle \approx 0.84\left|1s^2\right\rangle - 0.49\left|\left(6d_z^2\right)^2\right\rangle$, and it is just 0.06 eV lower than the $\widetilde{A}^3A_1$ state, $\left|\widetilde{A}^3A_1\right\rangle \approx 0.99\left|1s^1\left(6d_z^2\right)^1\right\rangle$. The singlet state can be seen as a mixture of a closed-shell singlet $1s^2$ (49%) and an open-shell singlet $1s^1(6d_z{}^2)^1$ (51%). The percentages are estimated from the 0.84 and 0.49 coefficients [44].

Table 1. Electronic configurations (EC) and excitation energies ΔE (eV) for the lowest lying electronic states of $Th(NH_3)_8^{3+}$, $Th(12C4N)_2^{3+}$ and $Th(12C4O)_2^{3+}$ at the CASSCF and CASPT2 levels of theory.

State	EC	CASSCF	CASPT2	CASSCF	CASPT2	CASSCF	CASPT2
		$\Delta E[Th(NH_3)_8^{3+}]$		$\Delta E[Th(12C4N)_2^{3+}]$ [a]		$\Delta E[Th(12C4O)_2^{3+}]$ [a]	
$\widetilde{X}^2A_1$	$(6d_z^2)^1$	0.00	0.00	0.00	0.00	0.00	0.00
1^2E_2	$(6d_{xy})^1/(6d_{x^2-y^2})^1$	1.35	1.28	1.03/1.05	1.04/1.02	1.61/1.29	1.57/1.27
1^2E_3	$(6d_{xz})^1/(6d_{yz})^1$	1.92	1.79			4.36/4.00	4.28/3.88
1^2B_2	$(7f_{z^3})^1$	2.08	1.94	2.03	2.03	N/C [b]	N/C [b]
1^2E_1	$(7f_{xz^2})^1/(7f_{yz^2})^1$	2.18	2.01	2.13/2.11	2.11/2.11	N/C [b]	N/C [b]
2^2A_1	$(1s)^1$	2.15	2.05	3.03	2.76	3.15	3.06
2^2B_2	$(1p_z)^1$	3.19	3.10			3.73	3.60
2^2E_1	$(1p_x)^1/(1p_y)^1$	3.24	3.15	3.50/3.36	3.23/3.10	3.42/3.71	3.36/3.64
2^2E_2	$(7f_{xyz})^1/(7f_{z(x^2-y^2)})^1$	3.30	3.18	3.24/3.26	3.22/3.25	N/C [b]	N/C [b]
2^2E_3	$(7f_{x(x^2-3y^2)})^1/(7f_{y(3x^2-y^2)})^1$	3.59	3.51	1.89/1.83	1.88/1.84	N/C [b]	N/C [b]
3^2A_1	$(1d_z^2)^1$	4.24	4.20			3.95	3.82
3^2E_2	$(1d_{x^2-y^2})^1/(1d_{xy})^1$	4.46	4.40			4.29/4.26	
3^2E_3	$(1d_{xz})^1/(1d_{yz})^1$	4.89	4.86				

[a] The degenerate states split into the $^2A/^2B$ components (C_2 point group; see text). [b] The assignment was not clear, since the 7*f* orbitals are highly mixed. The CASSCF/CASPT2 energies are 1.94, 2.09, 2.35, 2.37, 2.53, 3.55, 3.72/1.93, 2.09, 2.31, 2.34, 2.49, 3.49, 3.67 eV.

The next electronic states ($^{1,3}B_2$, $^{1,3}E_1$) lie between 0.72 and 0.93 eV and include all combinations of $1s^1 1p^1$ and $(6d_z^2)^1 1p^1$. The first $^{1,3}E_2$ states follow at 1.28 eV with configurations $1s^1(f/d)^1$ and $(6d_z^2)^1 1(f/d)^1$, where *f*/*d* refers to the orbitals produced from mixing 7*f*/6*d* orbital functions. We calculated ten more states, where electrons are promoted to outer 1d orbitals and Th 7*f* orbitals: 1.33 ($^1A_1$), 1.43 ($^1A_1$), 1.75 ($^1A_1$), 1.76 ($^3E_3$), 1.80 ($^1E_1$), 1.82 ($^3E_2$), 1.83 ($^3A_1$), 1.85 ($^1E_2$), 1.89 ($^3E_1$), 1.90 ($^1E_3$) eV.

Upon adding one more electron to form $Th(NH_3)_8^{1+}$, the ground state $\widetilde{X}^2A_1$ still has two major configurations involving the 1s and $6d_z^2$ orbitals, $\left|\widetilde{X}^2A_1\right\rangle \approx 0.84\left|\left(6d_z^2\right)^1 1s^2\right\rangle - 0.34\left|\left(6d_z^2\right)^2 1s^1\right\rangle$, comprising 71% and 12% of the wave function, respectively. Next, four quasi-degenerate states (two quartet and two doublet states) lie at 0.53 ± 0.03 eV (see Table 2). The quartets are single reference states with 95% of the wave function produced from some $(6d_z^2)^1 1s^1 1p^1$ configuration. The same percentages for the doublet states are 45% (1^2E_1) and 41% (1^2B_2) after adding the contribution from all three Slater determinants with different spin-up/spin-down combinations of $(6d_z^2)^1 1s^1 1p^1$. The next-largest term (34% for 1^2E_1 and 37% for 1^2B_2) corresponds to the $1s^2 1p^1$ configuration, which has three diffuse outer electrons, and finally a 15% portion (for both 1^2E_1 and 1^2B_2) belongs to $(6d_z^2)^2 1p^1$, where there is only one outer diffuse electron.

The above results were obtained with a $3e^-/10$ orbital active space, with the 10 orbitals being the $6d_z^2$, 1s, 1p, and 1d. According to these calculations, the higher-energy states are extremely multi-reference lying above 1.0 eV at the CASSCF level of theory. Compared to the dicationic and tricationic species, $Th(NH_3)_8^{1+}$ has a higher density of low-lying electronic states with five states in the first 0.6 eV. Only one or two states are present in this energy range for $Th(NH_3)_8^{3+}$ and $Th(NH_3)_8^{2+}$. Finally, as noted for the trication, the CASSCF and CASPT2 excitation energies are also in perfect agreement here (within 0.04 eV).

Moving to the neutral species ($4e^-/10$ orbitals), the fourth valence electron occupies a 1p orbital, resulting in the $(6d_z^2)^1 1s^2 1p^1$ configuration of the $\widetilde{X}^3E_1$ ground state, which is 72% of the wave function. This state is comparable to the addition of a 1p electron to $(6d_z^2)^1 1s^2$, the major component of ground state $\widetilde{X}^2A_1$ in $Th(NH_3)_8^{1+}$. The other component of $\widetilde{X}^2A_1$ is a $(6d_z^2)^2 1s^1$; addition of a 1p electron to this configuration constitutes only 2% of the ground state for $Th(NH_3)_8^0$. The $1p_{x,y}$ orbitals are populated first and the corresponding singlet and triplet states ($^{1,3}E_1$) are practically degenerate (see Table 2). The states $1^{1,3}B_2$ pertain to occupation of $1p_z$ and are higher by <0.1 eV.

Table 2. Electronic configurations (EC) and excitation energies ΔE (eV) for the lowest-lying electronic states of $Th(NH_3)_8^{1+}$ and $Th(NH_3)_8^{0}$ at the CASSCF and CASPT2 levels of theory.

State	Electron Configuration	ΔE (CASSCF)	ΔE (CASPT2)
	$Th(NH_3)_8^{1+}$		
$\widetilde{X}^2A_1$ [a]	$(6d_z^2)^1 1s^2/(6d_z^2)^2 1s^1$	0.00	0.00
1^2E_1 [a]	$(6d_z^2)^1 1s^1 1p_{x,y}^1/1s^2 1p_{x,y}^1/(6d_z^2)^2 1p_{x,y}^1$	0.47	0.50
1^4B_2	$(6d_z^2)^1 1s^1 1p_z^1$	0.48	0.51
1^4E_1	$(6d_z^2)^1 1s^1 1p_{x,y}^1$	0.49	0.53
1^2B_2 [a]	$1s^2 1p_z^1/(6d_z^2)^2 1p_z^1/(6d_z^2)^1 1s^1 1p_z^1$	0.53	0.56
	$Th(NH_3)_8^{0}$		
$\widetilde{X}^3E_1$	$(6d_z^2)^1 1s^2 1p_{x,y}^1$	0.00	0.00
$\widetilde{X}'^1E_1$	$(6d_z^2)^1 1s^2 1p_{x,y}^1$	0.01	0.00
1^3B_2	$(6d_z^2)^1 1s^2 1p_z^1$	0.04	0.04
1^1B_2	$(6d_z^2)^1 1s^2 1p_z^1$	0.11	0.09
1^3A_2	$(6d_z^2)^1 1s^1 1p_x^1 1p_y^1$	0.28	0.30
1^5A_2	$(6d_z^2)^1 1s^1 1p_x^1 1p_y^1$	0.27	0.31
1^5E_3	$(6d_z^2)^1 1s^1 1p_z^1 1p_{x,y}^1$	0.32	0.36
1^3E_3	$(6d_z^2)^1 1s^1 1p_z^1 1p_{x,y}^1$	0.38	0.39
1^1E_2 [a,b]	$(6d_z^2)^1 1s^1 1p^2/(6d_z^2)^1 1s^2 (1d_{xy,x^2-y^2})^1$	0.56	0.54
1^3E_2 [a,b]	$(6d_z^2)^1 1s^1 1p^2/(6d_z^2)^1 1s^2 (1d_{xy,x^2-y^2})^1$	0.55	0.56
1^1E_3 [a,b]	$(6d_z^2)^1 1s^1 1p^2/(6d_z^2)^1 1s^2 (1d_{xz,yz})^1$	0.63	0.60
2^3E_3 [a,b]	$(6d_z^2)^1 1s^1 1p^2/(6d_z^2)^1 1s^2 (1d_{xz,yz})^1$	0.63	0.62
1^3A_1 [a,b]	$(6d_z^2)^1 1s^1 1p^2/(6d_z^2)^1 1s^2 (1d_z^2)^1$	0.63	0.63
1^1A_1 [a,b]	$(6d_z^2)^1 1s^1 1p^2/(6d_z^2)^1 1s^2 (1d_z^2)^1$	0.65	0.63

[a] See text for percentages of each configuration. [b] The $1p^2$ configuration is in a singlet spin multiplicity; see text for more details.

The next batch of electronic states, $1^{3,5}A_2$ and $1^{3,5}E_3$, have a $(6d_z^2)^1 1s^1 1p^2$ character by 72% (S = 1) and 92% (S = 2). In every case, the $1p^2$ electrons couple into a triplet spin state. All lie in the range between 0.30 and 0.39 eV (see Table 2). Coupling of the $1p^2$ electrons into a singlet spin multiplicity generates the largest portion (from 42% to 58%) of the last six states of Table 2. Resembling the ^1D state of carbon, there are five $1p^2$ components belonging to the E_2, E_3 and A_1 irreducible representations. The second-largest contribution to the wave function of these states (26–34%) pertains to $(6d_z^2)^1 1s^2 1d^1$, which also has five components of the same irreducible representations. The excitation energies for these six states are 0.54−0.63 eV. Overall, the neutral species have the most "dense" electronic spectrum, with 14 states present within 0.63 eV. As in the cation, no *6d* or *7f* orbital (excluding $6d_z^2$) is occupied within the states studied, as additional electrons (relative to Th^{3+}) favor occupation of the outer orbitals. The active space used is the same as in $Th(NH_3)_8^{1+}$ ($4e^-/10$ orbitals).

In all octacoordinated thorium complexes, there is one inner electron in $6d_z^2$, which is perturbed by the molecular skeleton in order to avoid all Th-N coordination bonds (see Figure 3). This orbital has a substantial metallic/non-bonding character. The other *6d* orbitals have some σ_{Th-N}^* anti-bonding character and are higher in energy by at least 1.3 eV (see Table 1). As such, the addition of further ammonia ligands is expected to destabilize the $6d_z^2$ orbital, as these must approach along the z-direction, inducing a similar anti-bonding character. This is evidenced by our study of $Th(NH_3)_{10}$, where the addition of two ammonia ligands results in the promotion of the $6d_z^2$ electron to an outer 1s or 1p orbital (see Figure 4).

Specifically, we performed multi-reference calculations for all $Th(NH_3)_{10}^{3+,2+,1+,0}$ species ($4e^-/10$ orbitals, $3e^-/14$ orbitals, $2e^-/9$ orbitals, $1e^-/9$ orbitals) and found the ground states of $Th(NH_3)_{10}^{1+,0}$ have no inner electrons. Instead, they adopt $1s^1 1p^2$ (S = 3/2) and $1s^2 1p^2$ (S = 1) configurations. The ground states of $Th(NH_3)_{10}^{2+,3+}$ retain a metallic electron; this electron occupies an orbital and is composed of a mixture of *6d*/*7f* orbitals in

order to minimize its amplitude along the Th-N bonds. However, the $6d/7f \rightarrow 1s^1$ excitation for $Th(NH_3)_{10}^{3+}$ occurs at 0.72 eV and for $Th(NH_3)_{10}^{2+}$ at 0.14 eV compared to 2.05 eV for $Th(NH_3)_8^{3+}$ These results illustrate how the decacoordinate complex destabilizes the metallic electronic states and favors the promotion of electrons to the outer orbitals. The CASSCF active space used for each system included (number of electrons/number of orbitals) 1/10, 2/14, 3/9, and 4/9 for $Th(NH_3)_{10}^{3+,2+,1+,0}$, respectively; at CASPT2, correlation of all NH_3 lone pairs was also included and the geometries used were of C_2 symmetry. Further, it appears that the displacement of the $6d_z^2$ electron to the periphery of the complex reduces the binding energy of the ninth and tenth ammonia ligands (see Figure 2).

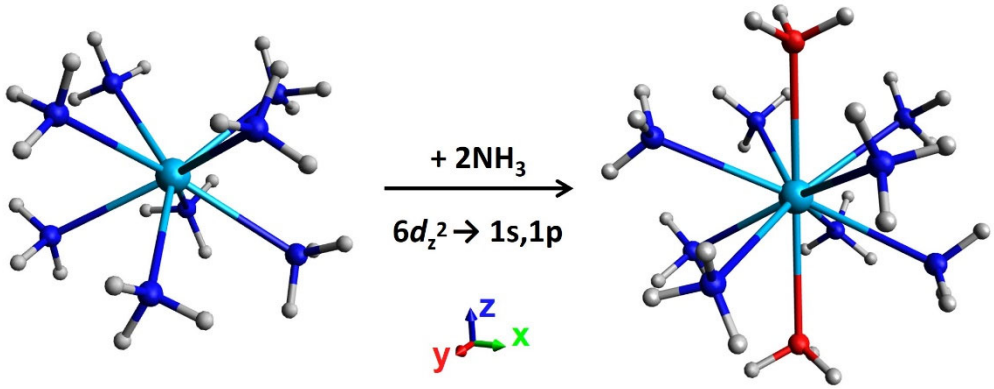

Figure 4. The addition of two ammonia ligands (marked with red nitrogen atoms) to the $Th(NH_3)_8^{3+,2+,1+,0}$ species occurs along the z-direction, resulting in the promotion of the $6d_z^2$ electron to an outer 1s or 1p orbital.

In an attempt to identify more stable complexes, we then studied the $Th(12C4N)_2$ and $Th(15C5N)_2$ aza-crown ethers (shown in Figure 5), where the "top" and "bottom" ammonia ligands of Figure 4 are connected via a hydrocarbon bridge with two carbon atoms (tetradentate ligands). Binding energies of the aza-crown ligands were calculated in two ways: (1) by dissociating the two ligands from Th, but keeping them fixed in the optimum geometry of the complex, and (2) by optimizing the dissociated ligands. For the constrained dissociation, the binding energy per Th-N bond in $Th(12C4N)_2^{4+,3+,0}$ is 114.0, 68.8, and 13.7 kcal/mol, respectively. The corresponding binding energies of the unconstrained geometry are 108.9, 63.7, and 8.6 kcal/mol. The drop in binding energy illustrates a steric strain introduced to the aza-crown rings during Th coordination of the order of ~5 kcal/mol. At CAM-B3LYP, the binding energy per Th-N bond in $Th(NH_3)_8^{4+,3+,0}$ is 103.5, 63.1, and 13.6 kcal/mol. From this, we see the energy of the 4+ and 3+ aza-crowns is comparable to that of the $Th(NH_3)_n^0$ complexes. However, the polydentate binding results in a more stable complex, as the removal of one aza-crown ligand is significantly more difficult, e.g., $4 \times 8.6 = 34.4$ kcal/mol. A similar situation is found for the $Th(15C5N)_2^{4+,3+,0}$ complexes: the per Th-N bond energies are 89.2, 53.2, and 12.2 kcal/mol for $Th(NH_3)_{10}^{4+,3+,0}$. The corresponding values for $Th(15C5N)_2^{4+,3+,0}$ are 93.0, 55.0, and 7.1 kcal/mol, respectively. Removal of one 15C5N ligand requires a minimum of 28.4 kcal/mol (4×7.1). In this case, we were able to obtain the CAM-B3LYP binding energies for all charges from 4+ to 0, which are listed in Table 3. This increased stability facilitates the formation of the neutral, decacoordinate Th complex, where it was unfavorable with ammonia ligands. This begs the question: How does the electronic structure change when replacing ammonia with aza-crown ethers, and does $Th(15C5N)_2$ have four peripheral electrons like $Th(NH_3)_{10}$?

To answer these questions, we performed CASSCF calculations. These were performed using the $Th(12C4N)_2^{4+}$ and $Th(15C5N)_2^{4+}$ optimized geometries, as they bear the highest possible symmetry (C_2 point group; see Figure 5 for the C_2 axis). Under this symmetry, the $1p_x$ and $1p_y$ orbitals remain quasi-degenerate, but the $1p_z$ is destabilized considerably and is not populated in the low-lying electronic states (see Figure 5 for the z-axis). The same happens for the 1d orbitals, where only the $1d_{xy}$ and $1d_{x^2-y^2}$ orbitals participate in

the low-lying states; all orbitals with amplitudes along the z-axis shift to higher energies, as has been seen for lithium–crown ether complexes [45]. Therefore, the active space has been adjusted to exclude these orbitals. Specifically, the active space used for the aza-crown ethers is (number of electrons/number of orbitals): 1/13, 2/8, 3/6, 4/6 and 1/15, 2/9, 3/6, 4/6 for $Th(12C4N)_2^{3+,2+,1+,0}$ and $Th(15C5N)_2^{3+,2+,1+,0}$, respectively.

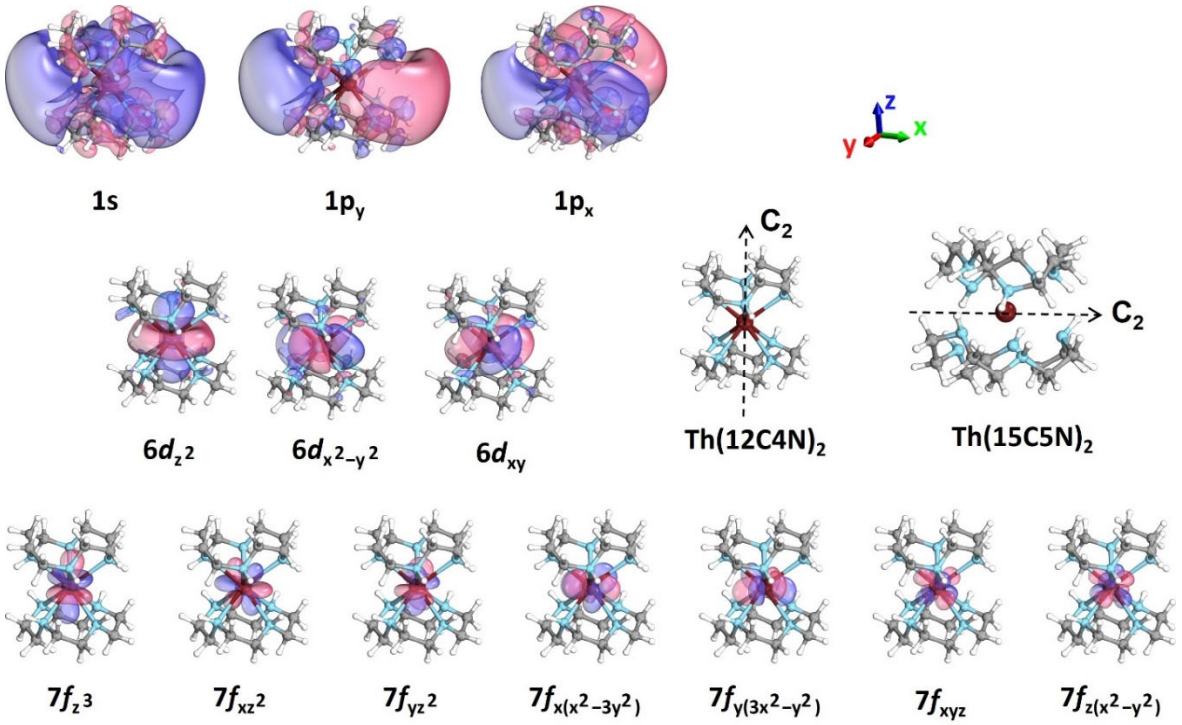

Figure 5. Geometries of $Th(12C4N)_2^{4+}$, $Th(15C5N)_2^{4+}$, and CASSCF active orbitals for $Th(12C4N)_2^{3+}$; 1s and 1p correspond to peripheral outer orbitals, and 6*d*, 7*f* to inner thorium orbitals.

Table 3. CAM-B3LYP binding energies per Th-N bond for thorium ammonia, thorium aza-crown ethers, and thorium crown ethers for various charges *q*.

q	$Th(NH_3)_8^q$	$Th(12C4N)_2^q$	$Th(12C4O)_2^q$	$Th(NH_3)_{10}^q$	$Th(15C5N)_2^q$	$Th(15C5O)_2^q$
+4	103.5	108.9	108.0	89.2	93.0	92.9
+3	63.1	63.7	64.1	53.2	55.0	54.9
+2	N/A	38.8	38.6	34.1	36.8	36.9
+1	N/A	19.3	18.7	19.1	15.4	14.2
0	13.6	8.6	6.1	12.2	7.1	5.1

The active orbitals and excitation energies for $Th(12C4N)_2^{3+}$ are given in Figure 5 and Table 1, respectively. Similarly to $Th(NH_3)_8^{3+}$, the ground state retains its $(6d_z{}^2)^1$ character and is still followed by the $(6d_{xy})^1/(6d_x{}^2{}_{-y}{}^2)^1$ states at around 1.04/1.02 eV (~0.3 eV lower). However, the inner $6d_{xz/yz}$ and outer $1p_z$ orbitals are no longer populated in the low-lying states, while the 1s outer orbital is polarized towards the xy plane. There are three reasons for these observed differences: (1) the Th^{4+} charge is less screened along the xy plane, (2) all N-H bonds (known to solvate electrons) point in the ±x/y directions, and (3) many of the C-H bonds (known to "repel" diffuse electrons) [5,25] point in the ±z directions. These effects shift the energy of the $1s^1$ state by ~0.7 eV from 2.05 to 2.76 eV. The $1p_{x,y}{}^1$ states are practically unaffected, and among the 1*f* orbitals, only the energy of the $(7f_{x(x}{}^2{}_{-3y}{}^2{}_{)})^1$ and $(7f_{y(3x}{}^2{}_{-y}{}^2{}_{)})^1$ states changes considerably, shifting from 3.59 to 1.86 ± 0.02 eV.

Going from $Th(12C4N)_2^{3+}$ to $Th(15C5N)_2^{3+}$, the overall picture remains the same, but now the inner $6d_{xz/yz}$ orbitals are populated and are highly mixed with the 7*f* ones.

It appears that the larger ring provides more space along the xz/yz diagonals, lowering the energy of the $6d_{xz/yz}{}^1$ states. This is the reason that the active space of $Th(15C5N)_2{}^{3+}$ includes two more orbitals (see above). These nine states (seven $7f^1$ + two $6d_{xz/yz}{}^1$) cover an energy range between 1.48 and 3.08 eV. The $(6d_{xy})^1/(6d_{x^2-y^2})^1$ states are located at 1.18/1.22 eV, and the outer $1s^1$ and $1p_{x,y}{}^1$ states move to 3.23 and 3.44/3.52 eV (~0.4 and ~0.2 eV higher). In all the three complexes $Th(NH_3)_8{}^{3+}$, $Th(12C4N)_2{}^{3+}$, and $Th(15C5N)_2{}^{3+}$ CASPT2 (vs. CASSCF) stabilizes the $1s^1$ and $1p^1$ states by about 0.3 eV.

The ground state of the dicationic thorium–aza-crown–ether complexes is a multi-reference singlet electronic state involving a mixture of $1s^2$, $(6d_z{}^2)^2$, and $1s^1(6d_z{}^2)^1$ configurations. This is followed by the single reference triplet $1s^1(6d_z{}^2)^1$ state. These states are 0.07 and 0.20 eV apart for $Th(12C4N)_2{}^{2+}$ and $Th(15C5N)_2{}^{2+}$, respectively. This mirrors the first two states of $Th(NH_3)_8{}^{2+}$. In $Th(NH_3)_8{}^{2+}$, the next states are six states with $1s^1 1p^1$ and $(6d_z{}^2)^1 1p^1$ character, but for the aza-crown ether complexes, only four of these states remain below 1.0 eV (0.28–0.38 eV for the tetra- and 0.59–0.71 eV for the penta-amine ligands), as the $1p_z$ orbital is highly destabilized.

The low-lying electronic states of the aza-crown monocationic complexes are identical to those of $Th(NH_3)_8{}^+$ (see Table 2) if we exclude the $^{2,4}B_2$ states, which populate the $1p_z$ orbital. The degeneracy of the $^{2,4}E_1$ states is lifted due to the lower symmetry: the two components of the doublet states are at 0.02/0.26 and 0.09/0.43 eV for $Th(12C4N)_2{}^+$ and $Th(15C5N)_2{}^+$, respectively, and those of the quartet states are at 0.04/0.29 and 0.14/0.57 eV.

Finally, for the neutral aza-crown complexes, only the states corresponding to $\widetilde{X}^3E_1$, $\widetilde{X}'^1E_1$, 1^3A_2, 1^5A_2, 1^1E_2, and 1^3E_2 of $Th(NH_3)_8$ (see Table 2) "survive", since the $1p_z$, $1d_z{}^2$, and $1d_{xz/yz}$ outer orbitals do not contribute. There are five nearly degenerate states within 0.03/0.13 eV for $Th(12C4N)_2/Th(15C5N)_2$. These are very multi-reference states (largest coefficient 0.48) with $(6d_z{}^2)^1 1s^2 1p_{x,y}{}^1$ and $(6d_z{}^2)^1 1s^1 1p_x{}^1 1p_y{}^1$ characters, with the ^3B always the ground state, followed by the ^1A (at 0.00/0.09 eV), ^1B (at 0.01/0.10 eV), ^3A (at 0.02/0.13 eV), and ^5B (at 0.03/0.12 eV) states. Notice the ^5B $[(6d_z{}^2)^1 1s^1 1p_x{}^1 1p_y{}^1]$ state is now closer to the ground state, since it has two electrons in the 1p orbitals, which are stabilized over 1s (see discussion on $Th(NH_3)_8{}^{3+}$ above and Table 1). The next four states are also highly multi-reference, involving the $(6d_z{}^2)^1 1s^1 1p^2$ and $(6d_z{}^2)^1 1s^2 (1d_{xy,x}{}^2{}_{-y}{}^2)^1$ configurations, and are located at 0.74–0.77/0.24–0.35 eV higher than the ground state.

To answer our earlier questions: the replacement of ammonia ligands with aza-crown ethers has a significant impact on the electronic structure and $Th(15C5N)_2$ has only three peripheral electrons, unlike $Th(NH_3)_{10}$, which has four. While $Th(NH_3)_{10}$ hosts four outer electrons ($1s^2 1p^2$) in the ground state, $Th(15C5N)_2$ favors the $(6d_z{}^2)^1 1s^m 1p_{x,y}{}^n$ ($m + n = 3$) configurations. The main reason is that two ammonia ligands are placed along the z-axis, which disfavors the presence of a $6d_z{}^2$ electron and promotes this electron to the outer 1s orbital (see Figure 4). The two neutral octa-coordination complexes, $Th(NH_3)_8$ and $Th(12C4N)_2$, have three outer electrons ($1s^2 1p^1$) and one inner $6d_z{}^2$ electron in their ground states. For the three reasons discussed above and symmetry lowering (D_{4d} to C_2), only the $1p_{x,y}$ and $1d_{xy,x}{}^2{}_{-y}{}^2$ (unlike $1p_z$ and $1d_z{}^2{}_{,xz,yz}$) participate in the low-lying states.

Finally, we performed calculations for the crown ether $Th(12C4O)_2{}^q$ and $Th(15C5O)_2{}^q$ (q = +4, +3, +2, +1, 0) complexes. Such complexes are the building units of electrides and our goal is to provide insights for electrides made of oxygen- and nitrogen-based crown ethers. Our CAM-B3LYP geometries and energies are listed in the Supplementary Materials and the binding energies are reported in Table 3. The per-bond binding energies are identical for the two kinds of ethers within the accuracy of our calculations.

Regarding the excited states of $Th(12C4O)_2{}^{3+}$, the electronic structure more closely resembles $Th(NH_3)_8{}^{3+}$ than $Th(12C4N)_2{}^{3+}$ owing to the greater equivalence of the z-direction to the x-,y-, as demonstrated by the relative energy of $1p_z{}^1$ to $1p_{x,y}{}^1$ (3.36, 3.60, 3.6 eV). The absence of the N-H bonds along the xy plane appears to make the space more isotropic. Calculated excitation energies are listed in Table 1 ($1e^-/20$ orbitals). The excited $6d$ states are higher in energy than those of $Th(NH_3)_8{}^{3+}$ and the $7f$ orbitals are highly mixed. The

outer 1s and 1p states are higher than the ammonia and aza-crown complexes, but the 1d states are in the same energy range as $Th(NH_3)_8^{3+}$.

The addition of an electron (CASSCF active space $2e^-/12$ orbitals) leads to two singlet states of $(6d_z^2)^2$ and $(6d_z^2)^1 1s^1$ mixed character at 0.00 and 0.43 eV, while the triplet $(6d_z^2)^1 1s^1$ state is located in between (0.21 eV). The next six states correspond to $(6d_z^2)^1 1p^1$. The three triplets have energies of 0.31, 0.43, 0.55 eV and the three singlets 0.43, 0.51, 0.56 eV. The addition of further electrons (CASSCF active spaces $3e^-/6$ orbitals, $4e^-/6$ orbitals) yields highly multi-reference wave functions. The ground state of $Th(12C4O)_2^{1+}$ is mainly $(6d_z^2)^1 1s^2$ followed by the $(6d_z^2)^1 1s^1 1p^1$ states lying between 0.04 and 0.18 eV, while the ground state of $Th(12C4O)_2$ is $(6d_z^2)^1 1s^2 1p^1$ followed by $(6d_z^2)^1 1s^1 1p^2$ states spanning an energy range of 0.05–0.25 eV. In every case, the low-lying states have only one inner electron and up to three outer electrons, similarly to the other complexes.

4. Conclusions

This work is the first systematic investigation of thorium SEPs. We used high-level electronic structure methods to study the thorium–ammonia, thorium–aza-crown, and thorium–crown ether complexes. We found that the octa-coordinate complexes are more stable, suggesting that the stoichiometry of thorium expanded metals will be $Th(NH_3)_8$. In all cases, except $Th(NH_3)_{10}$, there is a Th^{3+} center and zero/one $(1s^1)$/two $(1s^2)$/three $(1s^2 1p^1)$ outer electrons for 3+/2+/1+/0 charged complexes. In the case of $Th(NH_3)_{10}$ there is a Th^{4+} center with four diffuse electrons. The nature and energetics of the outer orbitals change considerably with the ligand type. Ammonia makes isotropic structures keeping the near degeneracy of the 1p and 1d orbitals. The aza-crown ethers have N−H bonds parallel to the crowns (xy dimension) and thus disfavor orbitals lying along the z-axis. The replacement of NH with O (plain metal–crown ether complexes) restores partially the isotropic environment, but increases the energy of the $1s^1$ and $1p^1$ states of the trications. For all species, although the $1s^1/1p^1$ states are higher in energy than $6d^1/7f^1$ states, they are populated first when at least a second electron is added. The wave functions become extremely multi-determinantal when two or more active electrons are present, and thus multi-reference methods are sine qua non for these systems. More work on other lanthanide/actinide complexes in the gas and condensed phases is in progress.

Supplementary Materials: The following supporting information can be downloaded at: https://www.mdpi.com/article/10.3390/molecules28124712/s1, Figure S1: Structures of aza-crown ether 12C4N: (a) fully optimized, (b) fixed at the geometry in the $Th(12C4N)_2^{4+}$ complex.; Table S1: Energies (hartrees) for the $Th(NH_3)_{n=0-10}^{4+,3+,0}$ species. The spin for the charged species is singlet (4+) and doublet (3+), while for the neutral species both the lowest singlet (S = 0) and triplet (S = 1) states are reported.; Table S2: Cartesian coordinates (Å) for the $Th(NH_3)_{n=1-10}^{4+,3+,0}$ species. The spin for the charged species is singlet (4+) and doublet (3+), while for the neutral species both the lowest singlet (S = 0) and triplet (S = 1) states are reported.; Table S3: Energies (hartrees) for the $Th(12C4X)_2^q$ and $Th(15C5X)_2^q$ species (q = 4+, 3+, 2+, 1+, 0 and X = N, O). Different spin states are reported (spin is given in parenthesis).; Table S4: Cartesian coordinates (Å) for the $Th(12C4X)_2^q$ and $Th(15C5X)_2^q$ species (q = 4+, 3+, 2+, 1+, 0 and X = N, O). Different spin states are reported (spin is given in parenthesis).

Author Contributions: Conceptualization, E.M.; methodology, E.M. and B.A.J.; software, E.M., B.A.J. and Z.L.; validation, E.M. and B.A.J.; investigation, E.M., B.A.J. and Z.L.; resources, E.M.; data curation, E.M.; writing—original draft preparation, E.M.; writing—review and editing, E.M. and B.A.J.; visualization, E.M.; supervision, E.M.; project administration, E.M. and B.A.J.; funding acquisition, E.M. All authors have read and agreed to the published version of the manuscript.

Funding: This work was funded by the United States Department of Energy–Basic Energy Sciences through the Chemical Sciences, Geosciences, and Biosciences (CSGB) subdivision for Heavy Elements Chemistry with Award DE-SC0019177, and the National Science Foundation under grant CHE-1940456.

Institutional Review Board Statement: Not applicable.

Informed Consent Statement: Not applicable.

Data Availability Statement: DFT/CAM-B3LYP geometries and energies for all structures are listed in Tables S1–S4 of the Supplementary Materials File.

Acknowledgments: The authors are indebted to Auburn University (AU) for financial support. EM is especially grateful to the donors of the James E. Land endowment, and Anne Elizabeth Gorden (Texas Tech University) for the valuable discussions. This work was completed with resources provided by the Auburn University Hopper and Easley Clusters. The authors would like to acknowledge the contributions of Jared Stinson for his assistance on the Th–crown ether complexes.

Conflicts of Interest: The authors declare no conflict of interest.

References

1. Ariyarathna, I.R.; Khan, S.N.; Pawłowski, F.; Ortiz, J.V.; Miliordos, E. Aufbau Rules for Solvated Electron Precursors: $Be(NH_3)_4^{0,\pm}$ Complexes and Beyond. *J. Phys. Chem. Lett.* **2018**, *9*, 84–88. [CrossRef]
2. Ariyarathna, I.R.; Pawłowski, F.; Ortiz, J.V.; Miliordos, E. Molecules mimicking atoms: Monomers and dimers of alkali metal solvated electron precursors. *Phys. Chem. Chem. Phys.* **2018**, *20*, 24186–24191. [CrossRef]
3. Almeida, N.M.S.; Pawłowski, F.; Ortiz, J.V.; Miliordos, E. Transition-metal solvated-electron precursors: Diffuse and 3d electrons in $V(NH_3)^{0,\pm}{}_6$. *Phys. Chem. Chem. Phys.* **2019**, *21*, 7090–7097. [CrossRef]
4. Ariyarathna, I.R.; Almeida, N.M.S.; Miliordos, E. Stability and Electronic Features of Calcium Hexa-, Hepta-, and Octa-Coordinated Ammonia Complexes: A First-Principles Study. *J. Phys. Chem. A* **2019**, *123*, 6744–6750. [CrossRef]
5. Jordan, Z.; Khan, S.N.; Jackson, B.A.; Miliordos, E. Can boron form coordination complexes with diffuse electrons? Evidence for linked solvated electron precursors. *Electron. Struct.* **2022**, *4*, 015001. [CrossRef]
6. Almeida, N.M.S.; Miliordos, E. Electronic and structural features of octa-coordinated yttrium–ammonia complexes: The first neutral solvated electron precursor with eight ligands and three outer electrons. *Phys. Chem. Chem. Phys.* **2019**, *21*, 7098–7104. [CrossRef]
7. Jackson, B.A.; Miliordos, E. Electronic and geometric structure of cationic and neutral chromium and molybdenum ammonia complexes. *J. Chem. Phys.* **2021**, *155*, 014303. [CrossRef]
8. Khan, S.N.; Miliordos, E. Scandium in Neutral and Positively Charged Ammonia Complexes: Balancing between Sc^{2+} and Sc^{3+}. *J. Phys. Chem. A* **2020**, *124*, 4400–4412. [CrossRef]
9. Takasu, R.; Misaizu, F.; Hashimoto, K.; Fuke, K. Microscopic Solvation Process of Alkali Atoms in Finite Clusters: Photoelectron and Photoionization Studies of $M(NH_3)_n$ and $M(H_2O)_n$ (M = Li, Li^-, Na^-). *J. Phys. Chem. A* **1997**, *101*, 3078–3087. [CrossRef]
10. Brockhaus, P.; Hertel, I.V.; Schulz, C.P. Electronically excited states in size-selected solvated alkali metal atoms. III. Depletion spectroscopy of $Na(NH_3)_n$-clusters. *J. Chem. Phys.* **1999**, *110*, 393–402. [CrossRef]
11. Lee, J.I.; Sperry, D.C.; Farrar, J.M. Spectroscopy and reactivity of size-selected Mg^+-ammonia clusters. *J. Chem. Phys.* **2004**, *121*, 8375–8384. [CrossRef]
12. Mune, Y.; Ohashi, K.; Iino, T.; Inokuchi, Y.; Judai, K.; Nishi, N.; Sekiya, H. Infrared photodissociation spectroscopy of $[Al(NH3)_n]+$ (n = 1–5): Solvation structures and insertion reactions of Al^+ into NH_3. *Chem. Phys. Lett.* **2006**, *419*, 201–206. [CrossRef]
13. Inoue, K.; Ohashi, K.; Iino, T.; Judai, K.; Nishi, N.; Sekiya, H. Coordination and solvation of copper ion: Infrared photodissociation spectroscopy of $Cu^+(NH_3)_n$ (n = 3–8). *Phys. Chem. Chem. Phys.* **2007**, *9*, 4793–4802. [CrossRef]
14. Salter, T.E.; Ellis, A.M. Structures of Small $Li(NH3)_n$ and $Li(NH_3)_n+$ Clusters ($n = 1-5$): Evidence from Combined Photoionization Efficiency Measurements and ab Initio Calculations. *J. Phys. Chem. A* **2007**, *111*, 4922–4926. [CrossRef] [PubMed]
15. Inoue, K.; Ohashi, K.; Iino, T.; Sasaki, J.; Judai, K.; Nishi, N.; Sekiya, H. Coordination structures of the silver ion: Infrared photodissociation spectroscopy of $Ag^+(NH_3)_n$ (n = 3–8). *Phys. Chem. Chem. Phys.* **2008**, *10*, 3052–3062. [CrossRef]
16. Ohashi, K.; Inoue, K.; Iino, T.; Sasaki, J.; Judai, K.; Nishi, N.; Sekiya, H. A molecular picture of metal ion solvation: Infrared spectroscopy of $Cu^+(NH_3)_n$ and $Ag^+(NH_3)_n$ in the gas phase. *J. Mol. Liq.* **2009**, *147*, 71–76. [CrossRef]
17. Imamura, T.; Ohashi, K.; Sasaki, J.; Inoue, K.; Furukawa, K.; Judai, K.; Nishi, N.; Sekiya, H. Infrared photodissociation spectroscopy of $Co^+(NH_3)_n$ and $Ni^+(NH_3)_n$: Preference for tetrahedral or square-planar coordination. *Phys. Chem. Chem. Phys.* **2010**, *12*, 11647–11656. [CrossRef]
18. Koga, N.; Ohashi, K.; Furukawa, K.; Imamura, T.; Judai, K.; Nishi, N.; Sekiya, H. Coordination and Solvation of V^+ with Ammonia Molecules: Infrared Photodissociation Spectroscopy of $V^+(NH_3)_n$ (n=4–8). *Chem. Phys. Lett.* **2012**, *539–540*, 1–6. [CrossRef]
19. Albaqami, M.D.; Ellis, A.M. Infrared spectroscopy of $Ca(NH_3)_n$ complexes. *Chem. Phys. Lett.* **2018**, *706*, 736–740. [CrossRef]
20. Kozubal, J.; Heck, T.R.; Metz, R.B. Vibrational Spectroscopy of $Cr^+(NH_3)_n$ (n = 1–6) Reveals Coordination and Hydrogen-Bonding Motifs. *J. Phys. Chem. A* **2019**, *123*, 4929–4936. [CrossRef]
21. Seel, A.G.; Swan, H.; Bowron, D.T.; Wasse, J.C.; Weller, T.; Edwards, P.P.; Howard, C.A.; Skipper, N.T. Electron Solvation and the Unique Liquid Structure of a Mixed-Amine Expanded Metal: The Saturated Li–NH_3–$MeNH_2$ System. *Angew. Chem. Int. Ed.* **2017**, *56*, 1561–1565. [CrossRef]
22. Seel, A.G.; Zurek, E.; Ramirez-Cuesta, A.J.; Ryan, K.R.; Lodge, M.T.J.; Edwards, P.P. Low energy structural dynamics and constrained libration of $Li(NH_3)_4$, the lowest melting point metal. *Chem. Comm.* **2014**, *50*, 10778–10781. [CrossRef]
23. Glaunsinger, W.S.; Von Dreele, R.B.; Marzke, R.F.; Hanson, R.C.; Chieux, P.; Damay, P.; Catterall, R. Structures and properties of metal-ammonia compounds on the trail of a new ammonia geometry. *J. Phys. Chem.* **1984**, *88*, 3860–3877. [CrossRef]

24. Jackson, B.A.; Miliordos, E. Simultaneous CO_2 capture and functionalization: Solvated electron precursors as novel catalysts. *Chem. Comm.* **2022**, *58*, 1310–1313. [CrossRef]
25. Jackson, B.A.; Dale, S.G.; Camarasa-Gómez, M.; Miliordos, E. Introducing Novel Materials with Diffuse Electrons for Applications in Redox Catalysis and Quantum Computing via Theoretical Calculations. *J. Phys. Chem. C* **2023**, *127*, 9295–9308. [CrossRef]
26. Haynes, W.M. *CRC Handbook of Chemistry and Physics*, 93rd ed.; Taylor & Francis: Boca Raton, FL, USA, 2012.
27. Tutson, C.D.; Gorden, A.E.V. Thorium coordination: A comprehensive review based on coordination number. *Coord. Chem. Rev.* **2017**, *333*, 27–43. [CrossRef]
28. Blanchard, F.; Rivenet, M.; Vigier, N.; Hablot, I.; Grandjean, S.; Abraham, F. Solid State Chemistry of Ten-Fold Coordinate Thorium(IV) Complexes with Oxalates in the Presence of Ammonium and Hydrazinium Ions. *Cryst. Growth Des.* **2018**, *18*, 4593–4601. [CrossRef]
29. Ariyarathna, I.R. Superatomic Chelates: The Cases of Metal Aza-Crown Ethers and Cryptands. *Inorg. Chem.* **2022**, *61*, 579–585. [CrossRef] [PubMed]
30. Dunning, T.H. Gaussian basis sets for use in correlated molecular calculations. I. The atoms boron through neon and hydrogen. *J. Chem. Phys.* **1989**, *90*, 1007–1023. [CrossRef]
31. Kendall, R.A.; Dunning, T.H.; Harrison, R.J. Electron affinities of the first-row atoms revisited. Systematic basis sets and wave functions. *J. Chem. Phys.* **1992**, *96*, 6796–6806. [CrossRef]
32. Woon, D.E.; Dunning, T.H. Gaussian basis sets for use in correlated molecular calculations. IV. Calculation of static electrical response properties. *J. Chem. Phys.* **1994**, *100*, 2975–2988. [CrossRef]
33. Peterson, K.A. Correlation consistent basis sets for actinides. I. The Th and U atoms. *J. Chem. Phys.* **2015**, *142*, 074105. [CrossRef] [PubMed]
34. Weigand, A.; Cao, X.; Hangele, T.; Dolg, M. Relativistic Small-Core Pseudopotentials for Actinium, Thorium, and Protactinium. *J. Phys. Chem. A* **2014**, *118*, 2519–2530. [CrossRef] [PubMed]
35. Ariyarathna, I.R.; Pawłowski, F.; Ortiz, J.V.; Miliordos, E. Aufbau Principle for Diffuse Electrons of Double-Shell Metal Ammonia Complexes: The Case of $M(NH_3)_4@12NH_3$, M = Li, Be^+, B^{2+}. *J. Phys. Chem. A* **2020**, *124*, 505–512. [CrossRef] [PubMed]
36. Frisch, M.J.; Schlegel, G.W.T.H.B.; Scuseria, G.E.; Robb, M.A.; Cheeseman, J.R.; Scalmani, G.; Barone, V.; Petersson, G.A.; Nakatsuji, H.; Li, X.; et al. *Gaussian 16*; Gaussian, Inc.: Wallingford, CT, USA, 2016.
37. Ghigo, G.; Roos, B.O.; Malmqvist, P.A. A Modified Definition of the Zeroth-Order Hamiltonian in Multiconfigurational Perturbation Theory (CASPT2). *Chem. Phys. Lett.* **2004**, *396*, 142–149. [CrossRef]
38. Azizi, Z.; Roos, B.O.; Veryazov, V. How accurate is the CASPT2 method? *Phys. Chem. Chem. Phys.* **2006**, *8*, 2727–2732. [CrossRef]
39. Ariyarathna, I.R.; Miliordos, E. Geometric and electronic structure analysis of calcium water complexes with one and two solvation shells. *Phys. Chem. Chem. Phys.* **2020**, *22*, 22426–22435. [CrossRef]
40. Jackson, B.A.; Miliordos, E. The nature of supermolecular bonds: Investigating hydrocarbon linked beryllium solvated electron precursors. *J. Chem. Phys.* **2022**, *156*, 194302. [CrossRef]
41. Werner, H.-J.; Knowles, P.J.; Knizia, G.; Manby, F.R.; Schütz, M.; Celani, P.; Györffy, W.; Kats, D.; Korona, T.; Lindh, R.; et al. MOLPRO, Version 2015.1, a Package of ab Initio Programs. 2015. Available online: https://www.molpro.net/ (accessed on 5 June 2023).
42. Celani, P.; Werner, H.-J. Multireference perturbation theory for large restricted and selected active space reference wave functions. *J. Chem. Phys.* **2000**, *112*, 5546–5557. [CrossRef]
43. Roos, B.O.; Andersson, K. Multiconfigurational Perturbation-Theory with Level Shift—The Cr_2 Potential Revisited. *Chem. Phys. Lett.* **1995**, *245*, 215–223. [CrossRef]
44. Miliordos, E.; Ruedenberg, K.; Xantheas, S.S. Unusual Inorganic Biradicals: A Theoretical Analysis. *Angew. Chem. Int. Ed.* **2013**, *52*, 5736–5739. [CrossRef] [PubMed]
45. Ariyarathna, I.R.; Miliordos, E. Ground and excited states analysis of alkali metal ethylenediamine and crown ether complexes. *Phys. Chem. Chem. Phys.* **2021**, *23*, 20298–20306. [CrossRef] [PubMed]

Disclaimer/Publisher's Note: The statements, opinions and data contained in all publications are solely those of the individual author(s) and contributor(s) and not of MDPI and/or the editor(s). MDPI and/or the editor(s) disclaim responsibility for any injury to people or property resulting from any ideas, methods, instructions or products referred to in the content.